Universitat Autònoma de Barcelona

Dipòsit digital de documents de la UAB

This is the **accepted version** of the article:

Tatkiewicz, Witold I.; Seras-Franzoso, Joaquín; García Fruitós, Elena; [et al.]. «High-throughput cell motility studies on surface-bound protein nanoparticles with diverse structural and compositional characteristics». ACS Biomaterials Science & Engineering, Vol. 5, Issue 10 (October 2019), p. 5470-5480. DOI 10.1021/acsbiomaterials.9b01085

This version is available at https://ddd.uab.cat/record/233716

under the terms of the IN COPYRIGHT license

High-throughput cell motility studies on surface-bound protein nanoparticles with diverse structural and compositional characteristics

Witold I. Tatkiewicz,[1,2] Joaquin Seras-Franzoso,[2,3,4,£] Elena García-Fruitós,[2,3,4,„,&] Esther Vazquez,[2,3,4] Adriana R. Kyvik,[1,2] Nora Ventosa,[1,2] Judith Guasch,[1,2,5] Antonio Villaverde,[2,3,4] Jaume Veciana[1,2,] and Imma Ratera[1,2,*]*

[1] Department of Molecular Nanoscience and Organic Materials, Institut de Ciència de Materials de Barcelona (ICMAB-CSIC), Campus UAB, 08193 Bellaterra (Spain)

[2] CIBER de Bioingeniería, Biomateriales y Nanomedicina (CIBER-BBN), 08193 Bellaterra (Spain)

[3] Institut de Biotecnologia i de Biomedicina (IBB), Universitat Autònoma de Barcelona, 08193 Bellaterra (Spain)

[4] Departament de Genètica i de Microbiologia, Universitat Autònoma de Barcelona, 08193 Bellaterra (Spain)

[5] Dynamic Biomimetics for Cancer Immunotherapy, Max Planck Partner Group, ICMAB-CSIC, Campus UAB, 08193 Bellaterra (Spain)

Corresponding authors: vecianaj@icmab.es, iratera@icmab.es

KEYWORDS: Inclusion Bodies, cell motility, high throughput, tissue engineering, concentration gradients, surface patterning, protein nanoparticles

ABSTRACT. Eighty areas with different structural and compositional characteristics made of bacterial inclusion bodies formed by the fibroblast growth factor (FGF-IBs) were simultaneously patterned on a glass surface with an evaporation-assisted method that relies on the coffee-drop effect. The resulting surface patterned with these protein nanoparticles enabled to perform a high-throughput study of the motility of NIH-3T3 fibroblasts under different conditions including gradient steepness, particle concentrations and area widths of patterned FGF-IBs, using for the data analysis a methodology that includes "heat maps". From this analysis, we observed that gradients of concentrations of surface-bound FGF-IBs stimulate the total cell movement, but do not affect the total net distances travelled by cells. Moreover, cells tend to move towards an optimal intermediate FGF-IB concentration (i.e., cells seeded on areas with high IB concentrations moved towards areas with lower concentrations and vice versa reaching the optimal concentration). Additionally, a higher motility was obtained when cells were deposited on narrow and highly concentrated areas with IBs. FGF-IBs can be therefore used to enhance and guide cell migration, confirming that the decoration of surfaces with such inclusion body-like protein nanoparticles are promising biomaterials for regenerative medicine and tissue engineering.

1. INTRODUCTION

Control over cell motility has many practical applications in the field of tissue regeneration and tissue engineering in medical implants,[1] because cell migration is important for embryogenesis,[2-4] immune surveillance[5-6] and wound healing[7] among other biological processes. Although it is a universal ability and can be performed by all nucleated types of cells at a given point of their development, it is executed in various manners and, very often, specific conditions are required.[8] Indeed, cells operate within distinct contexts and respond to environments in different ways.[8] In vivo cell motility depends on both external factors and intrinsic properties of cells. External factors, provided by the extra-cellular matrix (ECM), operate at every stage of the movement cycle, stabilizing protrusions and maintaining the direction of migration.[9] Thus, cell shape and mobility are governed by the dimensionality of surface decoration (i.e., 3D, 2D, or 1D in case of a single fibre of collagen),[10-13] density and orientation of the ECM ligands (i.e., nanoscale or microscale structure of the ECM),[14-22] and stiffness (i.e., mechanical properties of the substrate).[23] Although many efforts have been done to reproduce in vitro the complex aspects of physiological conditions,[24] further advancements in nanofabrication and synthetic self-assembly are still needed.[1] One relevant achievement in this field was the establishment of protocols to generate in vitro gradients of soluble bioactive factors on surfaces.[25] There have emerged a few distinct techniques to produce gradients in controlled laboratory conditions on model substrates.[26-28] The combination of microfluidics[29] and immersion techniques[30] have become a successful approach for gradient generation and production of surface-bound gradients of such soluble molecules. Thus, various types of molecules have been used to form gradients for studying cell motility, such as chemokines,[31-32] antigens,[33] drugs,[18] RGD peptides,[34] proteins,[35] or calcium ions.[36] In these studies, the directionality of cell movement can be assessed,[37-38] by analyzing the directional persistence time (i.e., the time in which the cell movement persists in the same direction), the random motility coefficient (i.e., a coefficient analogous to a molecular diffusion coefficient) and the

chemotaxis index (i.e., a weighted ratio between the distance along a gradient and the total travelled distance). As examples of these studies we can mention the movement of *Dictyostelium discoideum* cells on PDMS substrates covered with various patterns of micropillars,[39] a standard assay to test a drug efficiency,[40] or cell movements in complex environments with chemical and topographical cues.[2] Nevertheless, the development of new biomaterials that can guide migration of target cells into the injury site, stimulate their growth and/or differentiation and degrade in response to matrix remodeling enzymes released by the cells during the progress of tissue repair, are still highly needed.[41] These biomaterials should be able to interact with specific adhesion and growth factor receptors expressed by target cells surrounding damaged tissues.

Recently, a positive impact of protein nanoparticles consisting of bacterial inclusion bodies (IBs) formed by fibroblast growth factors (FGF) on cell proliferation and guidance has been confirmed.[42-45] IBs are intriguing functional, protein-based materials produced by recombinant bacteria that have broad applications in catalysis, tissue engineering and biomedicine,[45] acting as stable depots of functional proteins.[46-47] With a regular pseudospherical shape and a size on the frontier of nano and micro scales, usually between 50 and 800 nm, these particles can be tailored to act as functional topographies in tissue engineering and regenerative medicine,[48] with a broad spectrum of emerging applications such as wound healing.[49] Surface-bound gradients of IBs consisting of the green fluorescence protein (GFP) have also been recently shown to influence cell motility.[50] Encouraged by the latter results, which were only based on physical cues (i.e., topography, geometry and roughness), we decided to study the effects of FGF-based IBs (FGF-IBs) that introduce a biochemical activity together with the physical cues to the substrate for promoting cell migration. Thus, cells not only could be stimulated by the topography of the substrate, but also by the biochemical activity of these inclusion body-like protein nanoparticles. More specifically, we planned to prepare simultaneously different patterns of FGF-IBs using a recently reported process based on an evaporation-assisted method

that relies on the coffee-drop effect.[50] In brief, the surface to be patterned is placed into a temperature-controlled cuvette filled with the nanoparticle suspension. Material deposition occurs locally on the three phase line where liquid-air interface meets the substrate surface and it is governed by a programmable peristaltic pump. This allows engineering surfaces with 2D custom concentration variations over large areas.

2. RESULTS AND DISCUSSION

Here we report the use of this device for preparing an orthogonally stripped inclusion body-like protein nanoparticles (FGF-IBs) pattern with gradients of controlled widths and heights as well as with controlled constant FGF-IBs nanoparticles concentrations on the same surface to perform high-throughput cell culture studies.

With the resulting patterned surface, we studied in the same experiment the influence of factors like: A) constant vs. gradient concentrations of FGF-IBs, B) the steepness of the FGF-IB gradients, C) the different absolute concentrations of FGF-IBs, and D) the impact of broad vs. narrow paths, (i.e., cell movement constraining on cell motility (**Figure 1**) on cell migration). Thus, we account a high-throughput method enabling to investigate diverse factors influencing the cell motility in a fast way reducing the time and resources needed, as well as the batch-to-batch variability that sometimes occurs in the IB production.[51]

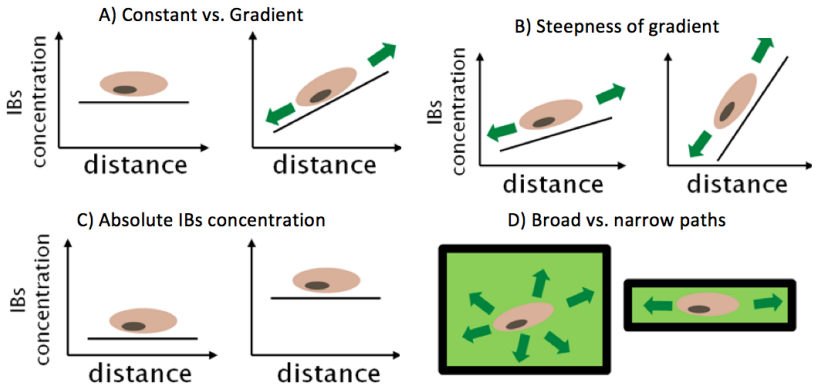

Figure 1. Scheme depicting the diverse parameters compared in the patterns of FGF-IBs and their influence on cell motility studied with the high-throughput methodology. A) Constant concentrations versus gradients, B) the steepness of gradients, C) absolute constant FGF-IB concentrations, and D) presence or absence of narrow paths. X and Y axes correspond to distance in the 200-500 μm range and concentrations in the range of 60,000- 150,000 IB/μm^2, respectively.

As shown before,[50] a surface with areas surrounded by concentrations of GFP-IBs higher than 500,000 particles·mm^{-2} deposits act as "corrals" for cell movement. Thus, using these high FGF-IB concentrations as cell barriers we patterned FGF-IBs consecutively in perpendicular directions on the same substrate using different deposition conditions (**Table 1**). In this way a patterned surface with 10 columns and 8 rows defining 80 areas with different FGF-IB concentrations and gradients were obtained in which each area is characterized by a unique combination of concentration (c_i) and gradient (d_i, h_i) parameters (**Figure 2**).

The patterned surface was obtained using a mixture containing 95% of FGF-IBs and 5% of GFP-IBs at a total concentration of $4.5 \cdot 10^{11}$ FGF-IB particles·ml^{-1}. The small percentage of GFP-IBs was used to visualize and identify the patterns by fluorescence microscopy and served as quality control measurement required for the multiple-iterations needed to develop the protocol for producing optimal gradients (**Figure 3** and section **S1** of SI).[28] We check that the presence of small amount (i.e., 5%) of GFP-IBs does not change the action of pure FGF-IBs in cell motility experiments performed with surfaces decorated with constant IB concentration.

The designed profile is not perfectly followed by the obtained substrate. However, the range of obtained slopes and concentration of deposited material is consistent over the entire deposition area, providing the prefect environment to study cell movement. The parameters describing the actual gradient's heights, lengths and slopes as well as the resulting concentrations of the 80 areas of the patterned surface are given in **Figure 2** and in section S1 of the SI.

The criteria to choose the dimensions of the grid follow the design proposed in **Figure 2** and **Table 1**. The design presents less distance for high steepness and higher distances for lower steepness. For a constant concentration, the dimension is constant. In general, for all the grids, the dimensions are big enough to be sure that the number of cells is enough to get statistically relevant data to be able to be evaluated without confluence.

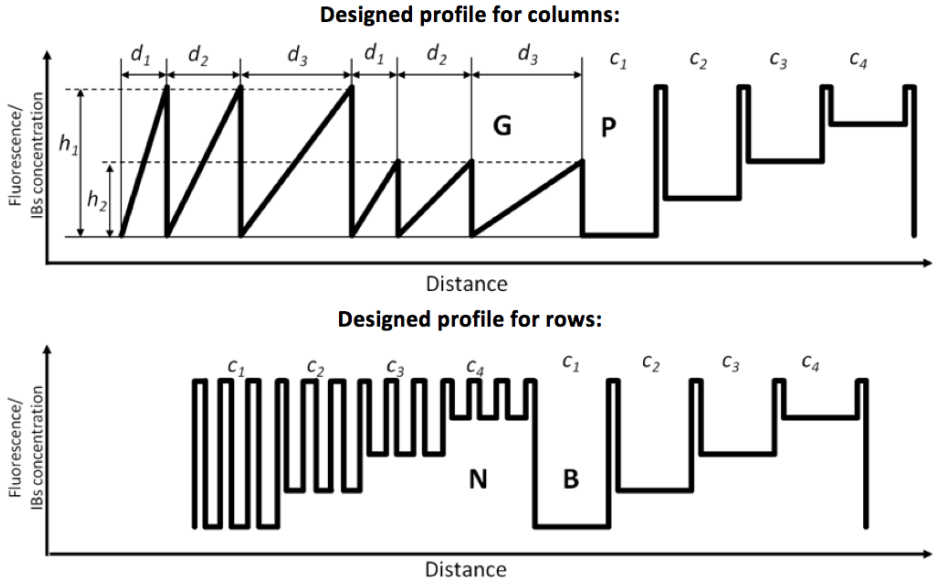

Figure 2. IB concentration profiles used to deposit FGF-IBs on the surface. The "column" profile consisted of 10 areas, each one with a different pattern (6 distinct gradients and 4 plain areas). Gradients are denoted with "G" and are characterized by their heights (*h*) and widths (*d*). Constant FGF-IB concentration areas, i.e. plain areas marked with "P" have various FGF-IB concentrations (c_i). The "row" profile consisted of 8 areas, 4 with narrow tracks "N" and 4 with broad areas "B". Each non-gradient subarea is characterized by 4 different FGF-IB concentration ($c_1 > c_2 > c_3 > c_4$). Concentrations (in thousands IBs per μm^2) c_1=66.8, c_2=92.5, c_3=93.7, c_4=150.2, heights (concentration at the peak of slope in thousands FGF-IBs per μm^2): h_1= 270.0, h_2=135, distances (in micrometers): d_1=200, d_2=400, d_3=500.

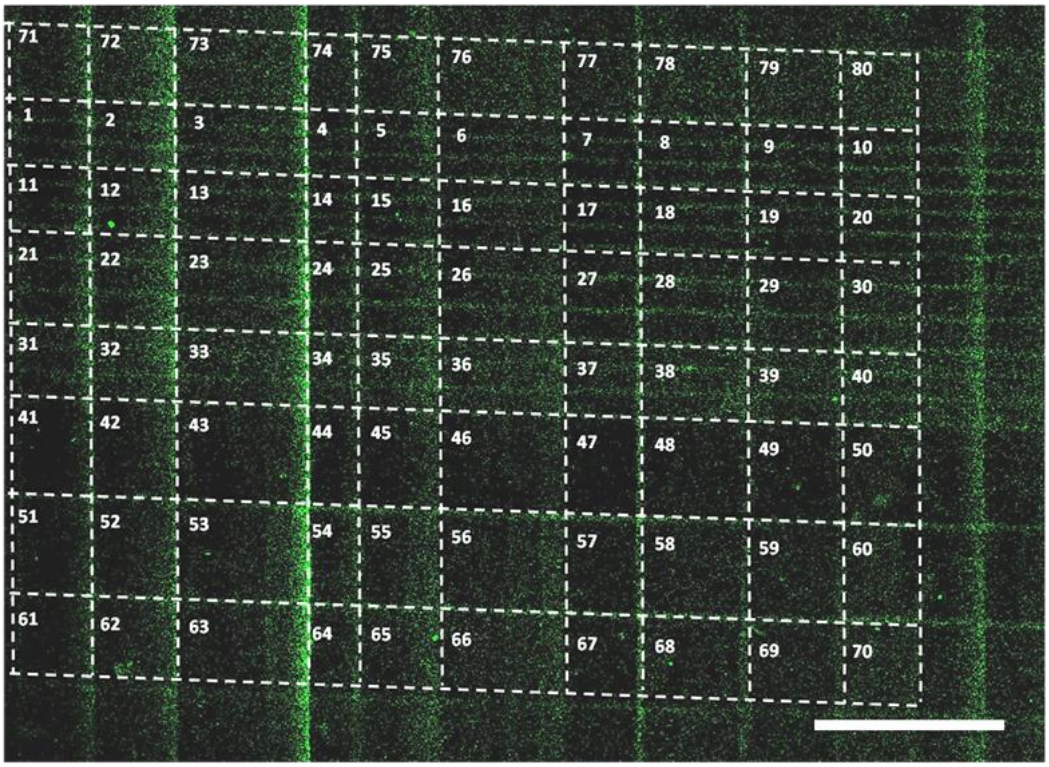

Figure 3. Confocal microscopy image of the substrate engineered with FGF-IBs for cell motility studies. The resulting 80 different areas are limited by white dashed lines. For convenience each area is marked with a number corresponding to **Table 1**. The image is cropped so that last row (areas 71-80) appears on top of the first row (areas 1-10). This aspect has no impact on the results, as the pattern has translational symmetry in 2D. Scale bar = 1 mm.

Table 1. Descriptors for FGF-IBs concentrations and gradients of the patterned surface. G: column with a concentration gradient, P: column with a constant concentration, named as plain area, N: row with narrow tracks, B: row with a broad area, *h*: gradient height, *d*: gradients width, *c*: FGF-IB concentrations ($c_1<c_2<c_3<c_4$). Each of the 80 areas has its unique descriptor (in black) and is characterized by the combination of parameters inherited from the columns (blue) and rows (red).

	G, d_1, h_1	G, d_2, h_1	G, d_3, h_1	G, d_1, h_2	G, d_2, h_2	G, d_3, h_2	P, c_1	P, c_2	P, c_3	P, c_4
	1	2	3	4	5	6	7	8	9	10
N, c_1	G, d_1, h_1	G, d_2, h_1	G, d_3, h_1	G, d_1, h_2	G, d_2, h_2	G, d_3, h_2	P, c_1	P, c_2	P, c_3	P, c_4
	N, c_1	N, c_1	N, c_1	N, c_1	N, c_1	N, c_1	N, c_1	N, c_1	N, c_1	N, c_1
	11	12	13	14	15	16	17	18	19	20
N, c_2	G, d_1, h_1	G, d_2, h_1	G, d_3, h_1	G, d_1, h_2	G, d_2, h_2	G, d_3, h_2	P, c_1	P, c_2	P, c_3	P, c_4
	N, c_2	N, c_2	N, c_2	N, c_2	N, c_2	N, c_2	N, c_2	N, c_2	N, c_2	N, c_2
	21	22	23	24	25	26	27	28	29	30
N, c_3	G, d_1, h_1	G, d_2, h_1	G, d_3, h_1	G, d_1, h_2	G, d_2, h_2	G, d_3, h_2	P, c_1	P, c_2	P, c_3	P, c_4
	N, c_3	N, c_3	N, c_3	N, c_3	N, c_3	N, c_3	N, c_3	N, c_3	N, c_3	N, c_3
	31	32	33	34	35	36	37	38	39	40
N, c_4	G, d_1, h_1	G, d_2, h_1	G, d_3, h_1	G, d_1, h_2	G, d_2, h_2	G, d_3, h_2	P, c_1	P, c_2	P, c_3	P, c_4
	N, c_4	N, c_4	N, c_4	N, c_4	N, c_4	N, c_4	N, c_4	N, c_4	N, c_4	N, c_4
	41	42	43	44	45	46	47	48	49	50
B, c_1	G, d_1, h_1	G, d_2, h_1	G, d_3, h_1	G, d_1, h_2	G, d_2, h_2	G, d_3, h_2	P, c_1	P, c_2	P, c_3	P, c_4
	B, c_1	B, c_1	B, c_1	B, c_1	B, c_1	B, c_1	B, c_1	B, c_1	B, c_1	B, c_1
	51	52	53	54	55	56	57	58	59	60
B, c_2	G, d_1, h_1	G, d_2, h_1	G, d_3, h_1	G, d_1, h_2	G, d_2, h_2	G, d_3, h_2	P, c_1	P, c_2	P, c_3	P, c_4
	B, c_2	B, c_2	B, c_2	B, c_2	B, c_2	B, c_2	B, c_2	B, c_2	B, c_2	B, c_2
	61	62	63	64	65	66	67	68	69	70
B, c_3	G, d_1, h_1	G, d_2, h_1	G, d_3, h_1	G, d_1, h_2	G, d_2, h_2	G, d_3, h_2	P, c_1	P, c_2	P, c_3	P, c_4
	B, c_3	B, c_3	B, c_3	B, c_3	B, c_3	B, c_3	B, c_3	B, c_3	B, c_3	B, c_3
	71	72	73	74	75	76	77	78	79	80
B, c_4	G, d_1, h_1	G, d_2, h_1	G, d_3, h_1	G, d_1, h_2	G, d_2, h_2	G, d_3, h_2	P, c_1	P, c_2	P, c_3	P, c_4
	B, c_4	B, c_4	B, c_4	B, c_4	B, c_4	B, c_4	B, c_4	B, c_4	B, c_4	B, c_4

Once the design and the preparation of the patterned substrate with FGF-IBs was successfully achieved, we used it to culture NIH-3T3 fibroblast cells, as model cells widely and recently used for tissue engineering applicability studies,[52-54] which were seeded at a density of 10.000 cells·cm^{-2} and studied their migration by time-lapse confocal microscopy (see **Figures S3** and **S4** in the SI).

The averaged total distance values travelled by the cells in each area and the distribution of such distances are presented in **Table 2** and **Figure 4**. Parameters defining the travelled distances by cells are given in **Figure S7** of the SI.

Table 2. Average total distance ($\bar{D}_{total}$ in μm) travelled by the cells in each area calculated for translations over a period of 22 h of image acquisition. Colors are added for classifying the $\bar{D}_{total}$ values in three ranges. Red, yellow, and green correspond to low (<270 μm), moderate (270-315 μm), and high (>315 μm) average total distances, respectively. The position of values in this table corresponds to the layout shown in **Table 1**.

Average total distance $\bar{D}_{total}$ [µm]		Gradient						Plain			
		High h_1			Low h_2						
		Narrow d_1	Moderate d_2	Broad d_3	Narrow d_1	Moderate d_2	Broad d_3	c_1	c_2	c_3	c_4
Narrow	c_1	256	304	364	306	294	243	233	295	231	246
	c_2	367	343	386	344	308	286	237	256	266	269
	c_3	304	361	361	318	282	312	260	236	336	280
	c_4	372	366	372	367	343	316	243	340	342	322
Broad	c_1	309	295	319	299	282	298	229	273	182	241
	c_2	309	334	322	280	310	302	250	241	247	250
	c_3	287	345	304	292	292	323	299	296	269	352
	c_4	307	323	252	256	320	268	297	280	328	272

A)

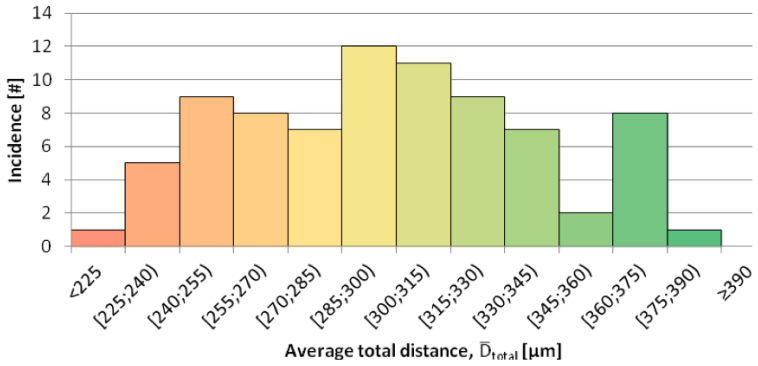

B)

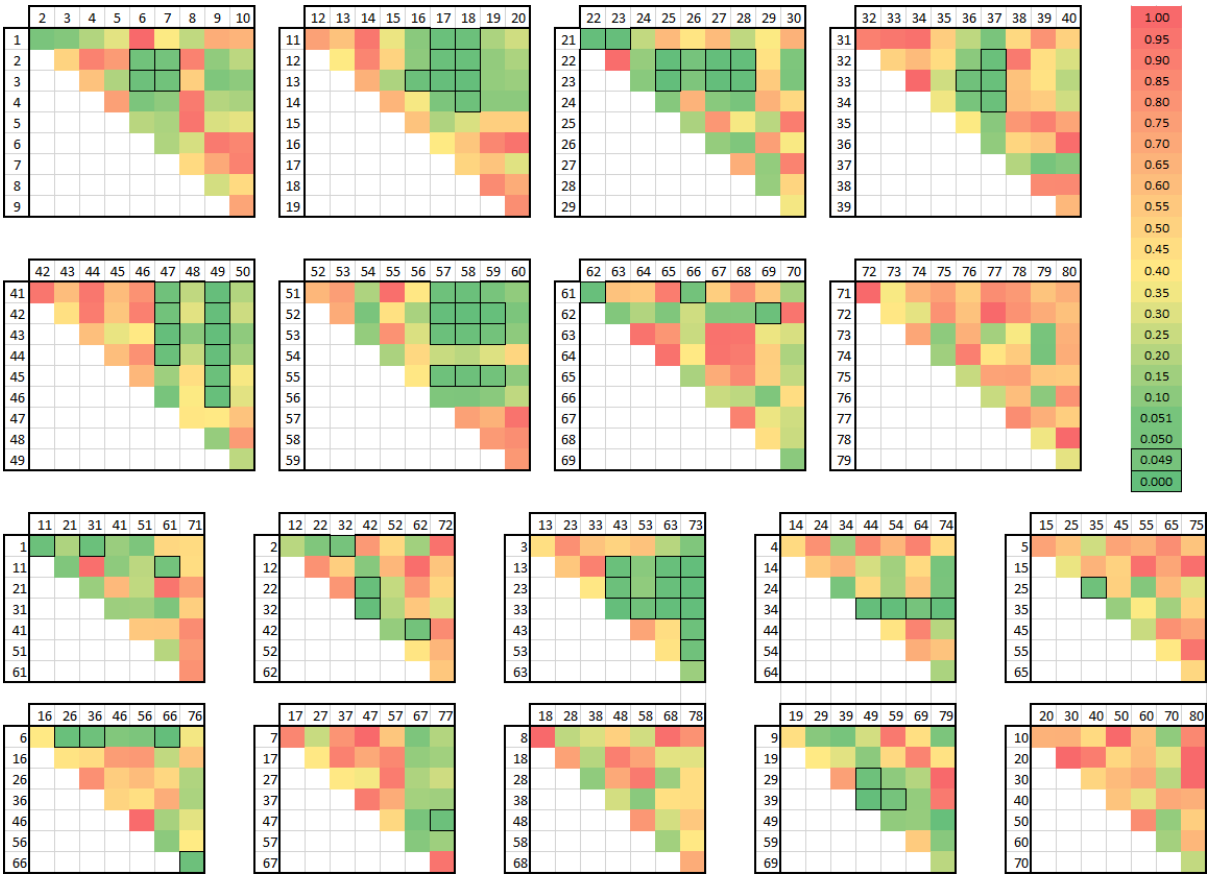

Figure 4. A) Distribution of average total distances, $\bar{D}_{total}$, travelled by cells in each area. This is the sum of all distances covered by cells during the experiment averaged by the number of cells in each area. A multimodal distribution can be observed with three distinct population of cells with low (<270 μm, red), medium (270-315 μm, yellow) and high (>315 μm, green) average total distances. B) Significance P-value heat map of non-parametric Kruskal-Wallis ANOVA test performed by pairs of areas. The total distance covered by cells in each one of the areas has been compared with the results obtained for cells in all the other areas. The indices on top and left of each table indicate which areas are compared, following the numbering of **Table1**. The colour of the squared bins at the intersection between areas indicates whether or not the difference is statistically significant between the two analysed areas. Green bins with borders denote pairs of areas where $p < 0.05$, (meaningful statistical difference). Yellow and red bins denote no statistically significant difference in cell movement. Only areas from the same row or column of **Table 1** are presented, as only these bins share at least one characteristic. A complete heat map is given in **Figure S3** of the SI. **Table S2** of SI shows the number of cells studied in each of the 80 areas.

The shortest distances were travelled by cells seeded over plain areas with constant FGF-IB concentrations. Indeed, these cells showed smaller migration distances than cells seeded on areas with gradients, especially when the gradients are steep. On the other hand, cell movement was further stimulated in narrow areas, tendency that was more pronounced in the FGF-IB gradient areas than in the plain ones.

Figure 4B shows that cell motility on areas with pattered gradients (areas X1-X6;) are significantly different than cells moving over areas with constant concentration (areas X7-X10); *i.e.* area 17 represent a cell behavior which is significantly different from area 11. The effect is even more pronounced for broad areas with low concentrations (areas 4X and 5X); i.e. area 53 represent a cell behavior which is significantly different from area 58. **Figure 4B** it also shows that gradient steepness' and the width of the areas does not influence cell motility when the total concentration of FGF-IB's is very high (areas 7X, 8X and X0); *i.e.* area 72 represent a cell behavior which is significantly different from area 80. It is worth mentioning that differences in motility are also statistically different for broad vs narrow areas (especially for areas X3); *i.e* area 13 represent a cell behavior which is significantly different from area 43.

This comparison can be easily visualized when the average values for each column or row are all juxtaposed (**Figure 5**). Thus, steeper gradients, and narrower areas promote larger cell

movements in a statistically significant manner. In contrast, high absolute concentrations of FGF-IBs on broad areas seem not to have impact on motility patterns in a statistically significant way. Thus, we can conclude that it is not the quantity of movement cues that trigger the significant differences, but their distribution on the micrometre scale.

Specifically, **Figure 5C** depicts that there is statistical difference in cell motility over gradient vs. plain areas, especially for steeper gradients (h_1). The slope has also impact on cell total distance (h_1 vs. h_2) for wider distances. It can also be observed that there is no significant difference between cell movement within plane areas or areas with calm slopes but steeper slopes do present statistically significant impact on cell behaviour.

Figure 5D show that there is statistically significant difference for cells moving within narrow areas in contrast to the broad ones where the absolute concentration does not have statistically significant impact on cell motility.

All above suggest that steep changes in cell environment (i.e. the presence of steep gradients, the presence of "corrals" in form of narrow areas) have more impact on cell motility than the absolute FGF-IBs concentration. Thus, it is not the quantity of movement cues that trigger this change, but their distribution on the micrometre scale.

In the next step, the averaged effective distance values travelled by cells, (i.e., the distance between the initial and the final cell position during the time-lapse imaging, see **Figure S7**), for each area were analyzed and results summarized on **Table 3.**

A)

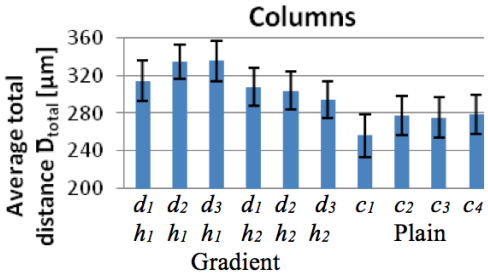

B)

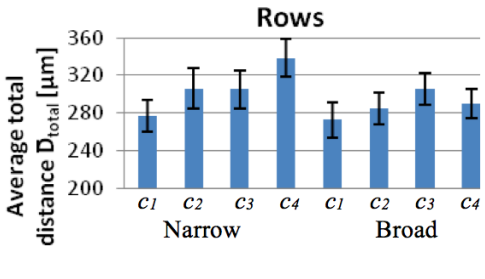

C) D)

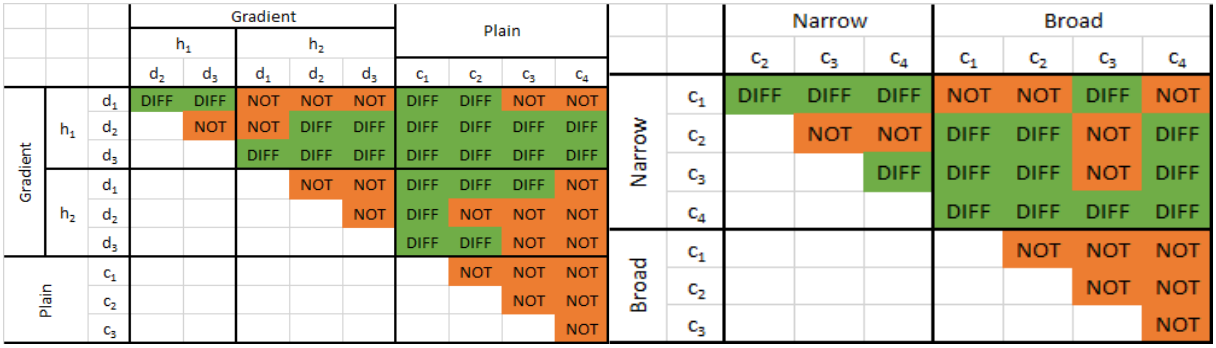

Figure 5. Summary of the averaged total distances from **Table 1** for a total number of n = 1462 cells. A) Histograms of total distances of cells where areas of the same columns (*i.e.* 1, 11, 21, …, 81) have been lumped into one population. Error bars indicate standard errors. B) Histograms of total distances of cells where areas of the same rows (*i.e.* 1, 2, 3, …, 10) have been lumped into one population. Error bars indicate standard errors. C) and D) present the statistical significance of total distances travelled by cells in each column or row, respectively. Populations were compared with each other using a pairwise Kruskall-Wallis ANOVA statistical analysis. Green and orange colour denote populations' behaviour which are statistically different ($p<0.05$) or not, respectively.

Table 3. Values of averaged effective distance ($\bar{D}_{eff}$ in μm) travelled by cells in each area. The position of values in this table corresponds to the layout presented in **Table 1**. The color code used is for group cells with low (<69 mm, in yellow), medium (60-90 mm, in orange) and high (>90mm, in green) average effective distances and they are in accordance with the color scale used in **Figure 4** assuming the same variation of both populations.

		Gradient						Plain			
		h_1			h_2						
		d_1	d_2	d_3	d_1	d_2	d_3	c_1	c_2	c_3	c_4
Narrow	c_1	67.3	66.8	85.9	71.8	73.9	59.0	61.5	105.5	44.3	70.3
	c_2	90.7	99.1	72.3	76.2	77.3	63.4	71.3	52.3	90.4	68.4
	c_3	58.9	80.3	72.8	61.0	56.2	56.5	50.0	66.3	89.0	51.7
	c_4	89.5	81.5	81.1	91.2	77.3	63.2	57.3	63.1	87.6	96.6
Broad	c_1	75.2	64.2	72.6	69.7	72.2	77.8	70.7	78.0	64.7	100.1
	c_2	67.5	72.3	81.1	80.3	62.3	60.9	62.2	35.7	59.3	71.5
	c_3	68.0	83.6	73.6	65.8	87.7	74.2	65.6	75.3	56.2	72.6
	c_4	105.5	46.2	51.5	47.3	60.3	38.1	93.4	80.7	59.7	61.0

The directionality of cell migration was also analyzed on the different patterned areas. Thus, the angle of cell movement, α_i, was defined as the angle between a reference horizontal line – parallel to direction of the patterning- and the line passing through the cell position on two consecutive confocal images (see **Figure S7** in the SI). Similarly, the effective angle, $\alpha_{effective}$, is given by the angle formed between the reference line and a line defined by the initial and final cell position (see **Figure S7** in the SI). The superposition of plots of partially pooled data from rows illustrated the preference of cells to move along the direction of narrow areas, given that a spindle-like distribution were obtained for cells in comparison with the random distributions found on broader areas (see **Figures 6** and **S7** and **S8** in SI). However, the average distributions for columns with high and low slope gradients as well as in the plain areas were similar. Thus, the presence or absence of gradients does not seem to influence cell directionality (**Figures 6** and **S7** and **S8** in SI).

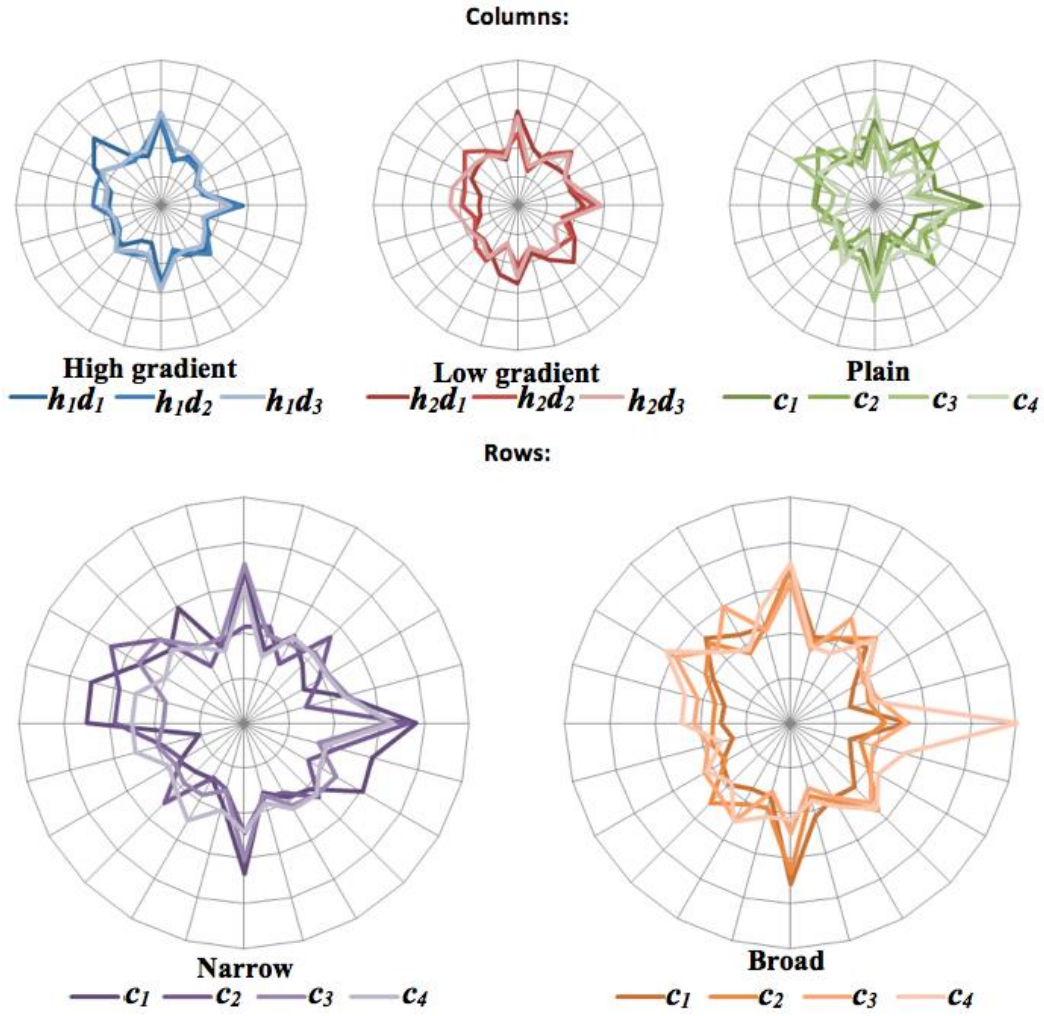

Figure 6. Momentary angular distributions calculated from the initial and final positions of cells during a 5 h cell migration experiment. Results were pooled for columns and rows and normalized with respect to cell number in each area (**Figure S4** and **Table S1** of SI).

To study how cells move inside the areas with FGF-IB concentration gradients we first determined the average local FGF-IB concentrations in all areas of the patterned substrate whose values are given **Table S1** and **Figure S2** of SI. Then, using time-lapse imaging we analyzed the movements of individual cells on each area along time finding that the migration did not show any clear trend, as exemplified for a few representative cases in **Figure S10** of SI. Thus, we decided to develop a method to analyze the data using the "probability heat maps" which provide information on the preferences of cells moving inside areas containing FGF-IB concentrations. To describe such "probability heat maps" we used the following notation in which the concentration of FGF-IBs around the cells at an initial position was denoted as x_i,

whereas the number of cells that moved from x_i to x_j, their final destination, was denoted as $n_{i,j}$. The latter value was divided by the total number of cells *Ni* (see **Table S2** and **S5** in the SI) at the studied area giving $n_{i,j}/N_i$ which describes the probability that a cell would move from a position with an FGF-IB concentration of x_i to another of x_j. Thus, a plot of $n_{i,j}/N_i$ for every final concentration x_j represents the probability to find cells at the final positions, i.e. to those positions where cells prefer to move starting from an initial point *i* with a given FGF-IB concentration of x_i (see **Figure S11** in the SI). This analysis highlights the preferences of cells moving within the patterned areas with different FGF-IB concentrations; thus allowing us to determine whether cells tend to move from low to high FGF-IB concentrations or vice versa. The resulting "probability heat maps" obtained for each area resembled tilted ovals, whose length (long axis along the diagonal) correspond to the range of FGF-IB concentrations present in each patterned area. If these areas had a gradient, cells could move within regions of both high and low FGF-IB concentrations and therefore the oval obtained was elongated along the diagonal. Conversely, the ovals of the plain areas are small, indicating that all concentrations were found within a narrow range, as expected. The width of an oval (short axis perpendicular to the diagonal) corresponds to the steepness of the gradients presented in the different areas. **Figure 7** presents a matrix of "probability heat maps" for all individual areas as well as their partial and total averages obtained for columns and rows, thus permitting us to visualize the movement of all analyzed cells at all times.

The main key finding is that the highest probabilities were obtained around the diagonal of each heat map, indicating that cells mostly move between points with very similar FGF-IB concentrations. However, every pixel outside the diagonal evidences that there were cells that changed their position between points of different FGF-IB concentrations, i.e. the farther the pixel from the diagonal, the larger the absolute difference between the FGF-IB concentration around the cell in the initial and final points. However, one of the key findings of the heat maps obtained is based on the symmetry of the matrix with respect to the diagonal which suggests

that the probability of a cell to move from a high to a low FGF-IB concentration area is the same than moving in the opposite direction.

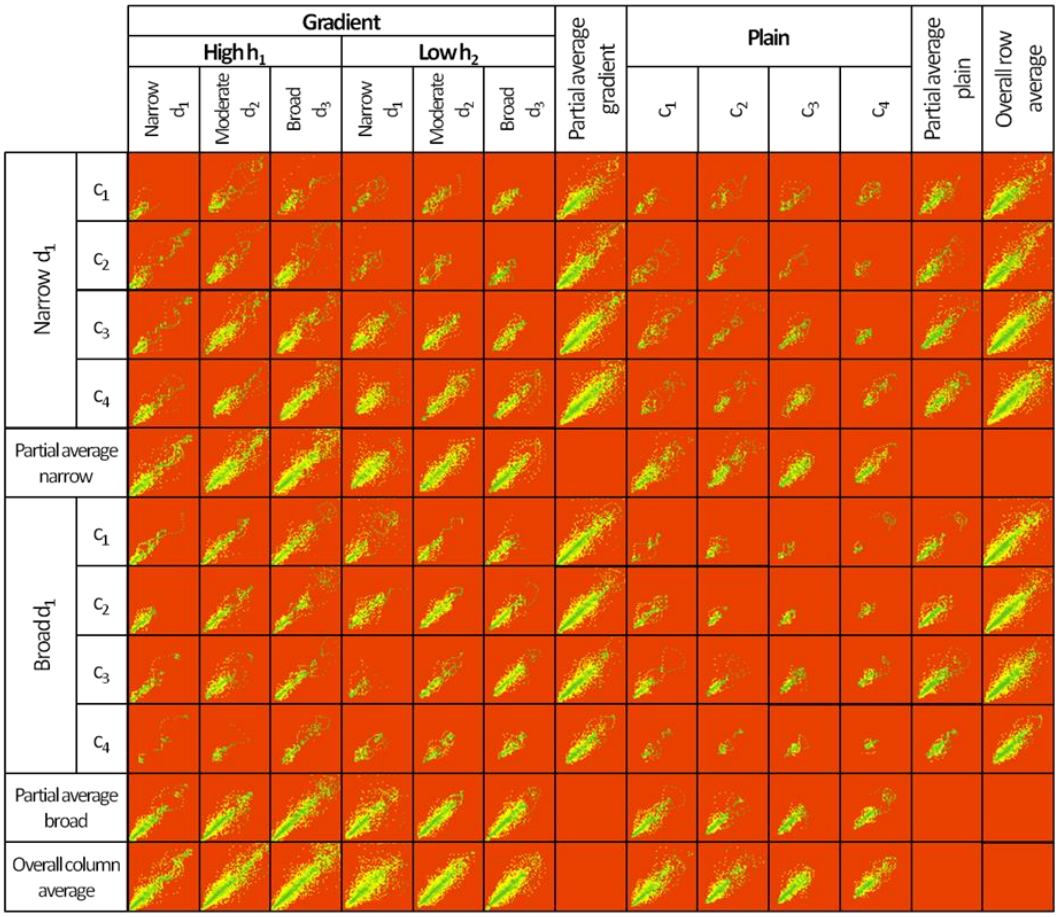

Figure 7. Matrix of "probability heat maps" for every area as well as the partial and total averages for columns and rows. Each heat map represents concentration range from 70,000 to 600,000 IBs/mm^2.

To confirm or reject the latter point another kind of matrix, named as "preference heat maps", were prepared (see **Figure S12** in the SI). In this representation, horizontal and vertical axis represented the initial x_i and the resulting x_j concentrations, respectively, as previously shown. However pixels held values of $(n_{i,j}/N_i)$-$(n_{j,i}/N_j)$ in order to compare the probability of cells shifting their position from a concentration of x_i to x_j with the probability of moving in the opposite direction, (i.e., from x_j to x_i, **Figure S12** in the SI). **Figure 8** shows the matrix of

"preference heat maps" of all individual areas as well as their partial and total averaged values obtained for columns and rows.

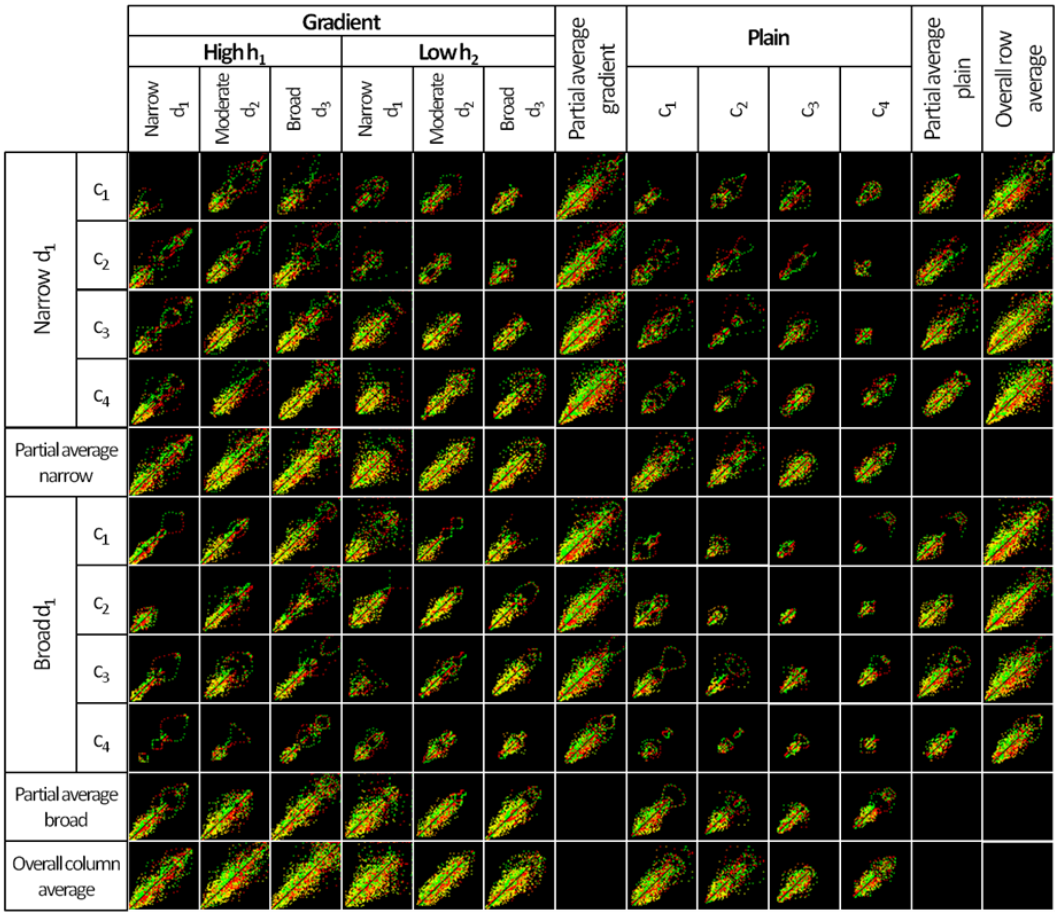

Figure 8. Matrix of "preference heat maps" for every area as well as partial and total averages for columns and rows. Each heat map represents concentration range from 70,000 to 600,000 IBs/mm^2.

Thus, the interpretation of the oval shapes is identical to the previous probability heat maps. However, in this case the color code denotes cell preferences. Given that these plots are diagonally anti-symmetric, the data represented above the diagonal is a mirror image of the data below it with reversed colors. The following analysis was therefore carried out using only one side of the ovals, specifically the one below the diagonal. In this part, green represented the preference of cells to move towards higher FGF-IB concentrations, red showed the preference of cells to move towards lower FGF-IB concentrations, yellow indicated that cells only present mild preferences, and black indicated no cell preferences or no data. A close examination of the

"preference heat maps" revealed that the coloring of the ovals followed a certain general simplified pattern shown in **Figure S13** in the SI. For low initial FGF-IB concentrations, there is a group of green pixels indicating that cells prefer to move towards higher concentrations. Moreover, the absence of colored pixels in the diagonal indicates that cells do not have a tendency to move towards areas of different concentrations. Alternatively, cells that are seeded on high initial FGF-IB concentrations preferred to move to lower concentrations, as shown by the red pixels close to the diagonal. These results are therefore suggesting that there is a preferred FGF-IB concentration that cells migrate until reached. This concentration is between 160,000 and 210,000 IBs/mm^2. Thus, 3T3 cells that were seeded on higher or lower concentrations of FGF-IBs than the optimal one, were migrating and ended up on areas within this range. Whereas cells that were already seeded over this optimal concentration spent the majority of their time in this range of concentrations.

Conversely, no clear influence of the steepness of the gradient on cell directionality was detected. These results are in agreement with our previous data, which showed that cells were freely moving inside corrals formed by IB-deposited surfaces surrounded by walls consisting of extremely high FGF-IB concentrations (500,000 particles/mm^2).[50]

3. CONCLUSIONS

In conclusion, we studied cell motility of fibroblasts in a high throughput manner, using a substrate that contained up to 80 different areas regarding structural and compositional characteristics, which was produced with a recently described method based on an evaporation-assisted methodology.[50] From such a study, we observed that gradient concentrations of surface-bound IBs stimulate total cell movement, but do not affect total net distances travelled by the cells. However, cells tend to move towards areas with an optimal IB concentration, *i.e.* cells seeded on high FGF-IB concentrations migrated to lower concentrations, whereas cells deposited on areas with low FGF-IB concentrations moved to areas with higher ones till

reaching an optimal concentration that range between 160,000 and 210,000 IBs/mm^2. Additionally, cells moved more when growing on narrower than broader areas, but the steepness of the gradient did not have a clear influence on the motility. This work demonstrates the use of a high-throughput method for a proper surface decoration with protein nanoparticles, such as FGF-IBs, which can be used to enhance and guide cell motility, confirming that FGF-IBs and its processing on surfaces is a promising biomaterial and platform to perform further experiments with primary cells towards applications in regenerative medicine as well as for tissue engineering.

4. MATERIALS AND METHODS

Preparation of Phosphate Buffered Saline (PBS) Solution. PBS is prepared by dissolving NaCl (5.494 g), Na_2HPO_4 (0.44 g), and NaH_2PO (0.108 g) in MilliQ water (1 l). Sodium hydroxide was used to obtain pH 7.4. Solution was diluted 10 times before use.

Bacterial Cells, Plasmids, and IB Production. The IBs are obtained and purified as previously described.[43] In summary, IBs were produced in the *E. coli* strain JGT20 (dnak756 thr::Tn10), a derivative of the pseudo-wild type MC4100. Bacterial cells were transformed with plasmid pTVP1GFP (ApR), coding an expressible green fluorescent protein (GFP) fusion. At its amino terminus, the fluorescent protein accommodates VP1, a hydrophobic structural protein from foot and-mouth disease virus. IBs formed by FGF were instead synthetized in *E. coli* BL21(DE3), from the plasmid vector pET29c- (þ)-hFGF-2. In both cases, gene expression was induced by culturing cells in shake flasks in LB medium and by adding 1 mM IPTG at 37 ºC (VP1GFP) and 25 ºC (FGF) at an OD550 of 0.5. Samples were taken 3 h after IPTG addition.

IB Purification. Lysozyme and PMSF at 1 mg/mL and 0.4 mM respectively were added to harvested bacterial cells, that were incubated for 2 h at 37 ºC. These mixtures were frozen at -

80 ºC to release IBs that were further washed in Triton X-100 1% (v/v) for 1 h at room temperature. After that, samples were frozen again at -80 ºC prior a secondary washing step with Nonidet P-40 0.03% (v/v) for 1 h at 4 ºC. Then, DNA was removed from IBs with 1 μg/mL DNase in 1 mM MgSO4 for 1 h at 37 ºC. Finally, IB preparations were frozen/thawed until no viable bacteria were observed.

Surface Modification. The surface to be patterned is modified to enhance IB deposition. A glass slide is cleaned using sonications in ethanol, utrapure water, and again ethanol. Then, the slides were exposed to vapors of hexamethyldisilazane (Sigma-Aldrich) for 12 h to obtain a hydrophobic surface.

Preparation and Characterization of IB Colloidal Suspensions.[28] Production and purification of GFP- and FGF-derived IBs was performed as previously described.[24b] IB aliquots were resuspended in Milli-Q water. The suspensions were sonicated for 10 min and left for 48 h at 4 °C. Then, the suspension was harvested discriminating the deposited sediment which consist of larger aggregates. Then, the storage suspension is diluted with Milli-Q water reaching the needed particle concentration. Before using, the suspensions were sonicated and degased for 10 min with argon. Nanoparticle tracking analysis (LM20 unit, Malvern Instruments) has been used to determine the concentration of particles (240 μg mL^{-1} or otherwise stated).

Device for Surface-Bound Gradient Deposition of pNPs from Colloidal Suspensions. The custom-made device has been designed to maximize the patterned area and minimize the volume of suspension needed (ca. 10 mL). Thus, a rectangular deposition cuvette with a very narrow cross section was used. Specifically, as previously described elsewhere, [28] the device consists of two planar polystyrene plates separated by a custom U-shaped polydimethylsiloxane (PDMS) seal attached to a metallic reservoir. This reservoir will be used to keep constant the temperature of the system. When compressed, a cuvette is obtained with dimensions big enough to introduce a cover glass of 50 × 25 mm. A hot plate is use during the deposition protocol to

keep homogeneous and constant de temperature (60 ± 3 °C). The temperature is keept higher than room T in order to increase the evaporation of the water but not enough to high to inactivate the IBs, as proven by the fluorescence images showing bright green fluorescence coming from the GFP-IBs. The top of the cuvette allows the access of the tube leading to the peristaltic pump that suction the water allowing to control the level of the colloidal suspension and thereby the contact line with the substrate to be patterned. The designed patterns are governed by the programmable peristaltic pump (Watson Marlow 403U/VM2) and its software (FIALab Instruments).

Nanoparticle Tracking Analysis (NTA): To quantify the FGF-IB concentration, 1.0 mL of aqueous suspensions were prepared by diluting the working suspensions (1:1000). Samples were measured at 298K with a LM20 unit (Nanosight, Malvern Instruments).

Cell cultures: NIH/3T3 cells (Sigma Aldrich) were routinely cultured in Dulbecco's modified Eagle medium (DMEM) supplemented with 2mM L-glutamine and 10% FBS (v/v) at 37ºC and 10% CO2 in a humidified incubator. 24 hours prior to cell seeding, the medium was switched to a low serum DMNM containing 1% FBS (v/v). Cells were then seeded at a concentration of 10000 cells/cm^2.

Time lapse imaging: The complete cell medium in a cultivation flask was changed to a cell medium with a 1% of serum 24 h prior to cell seeding over the sample in order to sensitize cells to the FGF content. In order to obtain confocal microscopy images, samples were mounted to an Attofluor cell chamber (A7816, Invitrogen). A Leica TCS SP5 AOBS spectral confocal microscope (Leica Microsystems) with a Plan-Apochromat 63x, 1.4 NA lens was used. GFP-IBs were excited with a 488 nm argon laser beam and detected at 500-537 nm. All the data that characterise cell positions originated from series of raw phase-contrast images captured every 30 min for 22 h.

Image treatment: Image treatment was carried out using ImageJ and its MTrackJ plugin (http://www.imagescience.org/meijering/software/mtrackj/). First, images were enhanced and

then cell positions were extracted from the time series. The average value of GFP fluorescence intensity was calculated for a circular area of ~2500 μm^2 around the position of cells. This value enabled to calculate the average FGF-IB concentration (and total concentration of IBs) under the cells and in their immediate surroundings.

Cell tracking: Cell, positions were captured using ImageJ ManulaTracking plugin. All the data that characterise cell positions originated from series of raw phase-contrast images captured every 30 min for 22 h.

Data treatment: Cell positions and corresponding average IB's concentration were extracted to MS Excel. Only cells that could be followed for at least 30 time points within one particular area, i.e. a period of 14.5 hours, and cells that moved a total distance over 100 μm were taken into account to perform the statistical analysis. Thus, cells that migrated from one area to another and other possible artifacts, (i.e., dead cells or impurities were excluded. Based on cell's position and image timestamp, speeds and orientations were calculated. Averages, standard errors, p-values from non-parametric Kruskal Wallis tests and other values that served as basis for further analyses and visualizations were calculated in MS Excel.

5. ACKNOWLEDGMENTS

This research was funded through DGI grants (MOTHER MAT2016-80826-R and Dynamo MAT2013-50036EXP), the Networking Research Center on Bioengineering, Biomaterials, and Nanomedicine (CIBER-BBN), the GenCat (grants 2017-SGR-918, 2017-SGR-229 and CERCA Programme), the COST Action CA15126 Between Atom and Cell, the European Social Fund and EU to J.V., A.V. and I.R. (H2020-INFRAIA-2014-2015; NFFA-654360). The authors are indebted to the Cell Culture Unit of the "Servei de Cultius Cel·lulars, Producció d'Anticossos i Citometria" (SCAC) and to the "Servei de Microscòpia", both at the UAB.

Protein NP production has been partially performed by the ICTS "NANBIOSIS", more specifically by the Protein Production Platform, Unit #1 (http://www.nanbiosis.es/unit/u1-protein-production-platform-ppp/) and by the Biomaterials Processing and Nanostructuring, Unit #6, (http://www.nanbiosis.es/portfolio/u6-biomaterial-processing-and-nanostructuring-unit/) of NANBIOSIS. W.I.T. is grateful to Consejo Superior de Investigaciones Científicas (CSIC) for a "JAE-pre" fellowship. J.S-F. is recipient of a Post-Doctoral fellowship from Asociación Española Contra el Cáncer (AECC), E.G-F. of a post-doctoral fellowship from INIA (DOC-INIA), and A.V. of an ICREA ACADEMIA award. This research was also supported by the People Programme (Marie Curie Actions) of the 7th Framework Programme of the European Union (FP7/2007-2013) under the grant agreement Nr. 600388 of REA and the Agency for Business Competitiveness ACCIÓ through a Tecniospring fellowship (TECSPR15-1-0015) to J.G. J.G. is also grateful to the Max Planck Society through the Max Planck Partner Group "Dynamic Biomimetics for Cancer Immunotherapy" in collaboration with the Max Planck Institute for Medical Research (Heidelberg, Germany). ICMAB acknowledges support from the Spanish Ministry of Economy and Competitiveness, through the ''Severo Ochoa'' Programme for Centres of Excellence in R&D (SEV-2015-0496).

ASSOCIATED CONTENT

Supporting Information. Characterization of surface-bond IB gradients and concentrations, snapshots of a time-lapse video of a migrating cell, number of studied cells in the cultured areas, parameters defining cellular migration distances and direction movements, heat maps construction.

AUTHOR INFORMATION

†Present address: Cibbim-Nanomedicine, Hospital Vall d'Hebron, Passeig de la Vall d'Hebron, 119-129, 08035, Barcelona, Spain

&Present address: Department of Ruminant Production, Institut de Recerca i Tecnologia Agroalimentàries (IRTA), 08140 Caldes de Montbui, Spain.

TABLE OF CONTENTS

High-throughput cell motility studies on surface-bound protein nanoparticles with diverse structural and compositional characteristics

Witold I. Tatkiewicz,[1,2] Joaquin Seras-Franzoso,[2,3,4,£] Elena García-Fruitós,[2,3,4,„,&] Esther Vazquez,[2,3,4] Adriana R. Kyvik,[1,2] Nora Ventosa,[1,2] Judith Guasch,[1,2,5] Antonio Villaverde,[2,3,4] Jaume Veciana[1,2,] and Imma Ratera[1,2,*]*

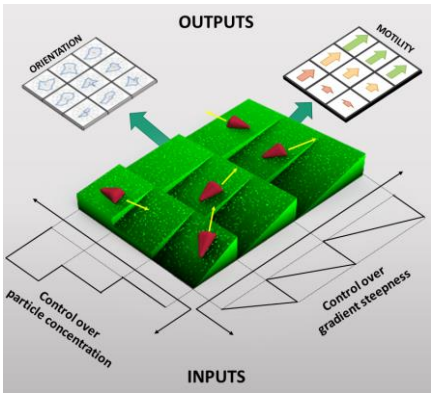

A high-throughput method for the simultaneous study of cell motility in a patterned surface with protein nanoparticles based on fibroblast growth factors exhibiting 80 areas with constant concentrations, concentration gradients of different steepness and narrow vs wide paths is presented.

KEYWORDS

Inclusion Bodies, cell motility, high-throughput, tissue engineering, concentration gradients, surface patterning, protein nanoparticles

REFERENCES

(1) Stevens, M. M.; George, J. H. Exploring and engineering the cell surface interface. *Science* **2005**, *310*, 1135-1138. 10.1126/science.1106587

(2) Solnica-Krezel, L.; Sepich, D. S. Gastrulation: making and shaping germ layers. *Annu. Rev. Cell Dev. Biol.* **2012**, *28*, 687-717. 10.1146/annurev-cellbio-092910-154043

(3) Reig, G.; Pulgar, E.; Concha, M. L. Cell migration: from tissue culture to embryos. *Development* **2014**, *141*, 1999-2013. 10.1242/dev.101451

(4) Concha, M. L.; Adams, R. J. Oriented cell divisions and cellular morphogenesis in the zebrafish gastrula and neurula: a time-lapse analysis. *Development* **1998**, *125*, 983-994.

(5) Lämmermann, T.; Germain, R. N. The multiple faces of leukocyte interstitial migration. *Semin. Immunopathol.* **2014**, *36*, 227-251. 10.1007/s00281-014-0418-8

(6) Lämmermann, T.; Bader, B. L.; Monkley, S. J.; Worbs, T.; Wedlich-Söldner, R.; Hirsch, K.; Keller, M.; Förster, R.; Critchley, D. R.; Fässler, R.; Sixt, M. Rapid leukocyte migration by integrin-independent flowing and squeezing. *Nature* **2008**, *453*, 51-55. 10.1038/nature06887

(7) *Actin-based motility (cellular, molecular and physical aspects);* Carlier, M.-F. Ed.; Springer Netherlands: Dordrecht, 2010. 10.1007/978-90-481-9301-1

(8) Friedl, P.; Wolf, K. Plasticity of cell migration: a multiscale tuning model. *J. Cell Biol.* **2010**, *188*, 11-19. 10.1083/jcb.200909003

(9) Petrie, R. J.; Doyle, A. D.; Yamada, K. M. Random versus directionally persistent cell migration. *Nat. Rev. Mol. Cell Biol.* **2009**, *10*, 538-549. 10.1038/nrm2729

(10) Sung, K. E.; Su, X.; Berthier, E.; Pehlke, C.; Friedl, A.; Beebe, D. J. Understanding the impact of 2D and 3D fibroblast cultures on in vitro breast cancer models. *PLOS One* **2013**, *8*, e76373. 10.1371/journal.pone.0076373

(11) Lepzelter, D.; Bates, O.; Zaman, M. Integrin clustering in two and three dimensions. *Langmuir* **2012**, *28*, 5379-5386. 10.1021/la203725a

(12) Li, Q.; Chow, A. B.; Mattingly, R. R. Three-dimensional overlay culture models of human breast cancer reveal a critical sensitivity to mitogen-activated protein kinase kinase inhibitors. *J. Pharmacol. Exp. Ther.* **2010**, *332*, 821-828. 10.1124/jpet.109.160390

(13) Pérez del Río, E.; Martinez Miguel, M.; Veciana, J.; Ratera, I.; Guasch, J. Artificial 3D culture systems for T cell expansion. *ACS Omega* **2018**, *3*, 5273-5280. 10.1021/acsomega.8b00521

(14) Guasch, J.; Diemer, J.; Riahinezhad, H.; Neubauer, S.; Kessler, H.; Spatz, J. P. Synthesis of binary nanopatterns on hydrogels for initiating cellular responses. *Chem. Mater.* **2016**, *28*, 1806-1815. 10.1021/acs.chemmater.5b04910
(15) Guasch, J.; Conings, B.; Neubauer, S.; Rechenmacher, F.; Ende, K.; Rolli, C. G.; Kappel, C.; Schaufler, V.; Micoulet, A.; Kessler, H.; Boyen, H.-G.; Cavalcanti-Adam, E. A.; Spatz, J. P. Segregation versus colocalization: orthogonally functionalized binary micropatterned substrates regulate the molecular distribution in focal adhesions. *Adv. Mater.* **2015**, *27*, 3737-3747. 10.1002/adma.201500900
(16) Rechenmacher, F.; Neubauer, S.; Mas-Moruno, C.; Dorfner, P. M.; Polleux, J.; Guasch, J.; Conings, B.; Boyen, H.-G.; Bochen, A.; Sobahi, T. R.; Burgkart, R.; Spatz, J. P.; Fässler, R.; Kessler, H. A molecular toolkit to functionalize Ti-based biomaterials that selectively control integrin-mediated cell adhesion. *Chem. Eur. J.* **2013**, *19*, 9218-9223. 10.1002/chem.201301478
(17) Comelles, J.; Caballero, D.; Voituriez, R.; Hortigüela, V.; Wollrab, V.; Godeau, A. L.; Samitier, J.; Martínez, E.; Riveline, D. Cells as active particles in asymmetric potentials: motility under external gradients. *Biophys. J.* **2014**, *107*, 1513-1522. 10.1016/j.bpj.2014.08.001
(18) Wu, A.; Loutherback, K.; Lambert, G.; Estévez-Salmerón, L.; Tlsty, T. D.; Austin, R. H.; Sturm, J. C. Cell motility and drug gradients in the emergence of resistance to chemotherapy. *Proc. Natl. Acad. Sci. U. S. A.* **2013**, *110*, 16103-16108. 10.1073/pnas.1314385110
(19) Maheshwari, G.; Brown, G.; Lauffenburger, D. A.; Wells, A.; Griffith, L. G. Cell adhesion and motility depend on nanoscale RGD clustering. *J. Cell Sci.* **2000**, *113*, 1677-1686.
(20) Ng, T.; Shima, D.; Squire, A.; Bastiaens, P. I. H.; Gschmeissner, S.; Humphries, M. J.; Parker, P. J. PKCα regulates β1 integrin-dependent cell motility through association and control of integrin traffic. *EMBO J.* **1999**, *18*, 3909-3923. 10.1093/emboj/18.14.3909
(21) Kyvik, A. R.; Luque-Corredera, C.; Pulido, D.; Royo, M.; Veciana, J.; Guasch, J.; Ratera, I. Stimuli-responsive functionalization strategies to spatially and temporally control surface properties: Michael vs. Diels alder type additions. *J. Phys. Chem. B* **2018**, *122*, 4481-4490. 10.1021/acs.jpcb.8b0165210.1021/acs.jpcb.8b01652
(22) Guasch, J.; Muth, C. A.; Diemer, J.; Riahinezhad, H.; Spatz, J. P. Integrin-assisted T-cell activation on nanostructured hydrogels. *Nano Lett.* **2017**, *17*, 6110-6116. 10.1021/acs.nanolett.7b02636

(23) Discher, D. E.; Janmey, P.; Wang, Y.-l. Tissue cells feel and respond to the stiffness of their substrate. *Science* **2005**, *310*, 1139-1143. 10.1126/science.1116995
(24) Griffith, L. G.; Swartz, M. A. Capturing complex 3D tissue physiology in vitro. *Nat. Rev. Mol. Cell Biol.* **2006**, *7*, 211-224. 10.1038/nrm1858
(25) Majumdar, R.; Sixt, M.; Parent, C. A. New paradigms in the establishment and maintenance of gradients during directed cell migration. *Curr. Opin. Cell Biol.* **2014**, *30*, 33-40. 10.1016/j.ceb.2014.05.010
(26) Chung, B. G.; Manbachi, A.; Saadi, W.; Lin, F.; Jeon, N. L.; Khademhosseini, A. A gradient-generating microfluidic device for cell biology. *J. Vis. Exp.* **2007**, *7*, e271. 10.3791/271
(27) Kim, S.; Kim, H. J.; Jeon, N. L. Biological applications of microfluidic gradient devices. *Integr. Biol.* **2010**, *32*, 584-603. 10.1039/c0ib00055h
(28) Li, S.; Guan, J.-L.; Chien, S. Biochemistry and biomechanics of cell motility. *Annu. Rev. Biomed. Eng.* **2005**, *7*, 105-150. 10.1146/annurev.bioeng.7.060804.100340
(29) Cho, H.; Hamza, B.; Wong, E. A.; Irimia, D. On-demand, competing gradient arrays for neutrophil chemotaxis. *Lab Chip* **2014**, *14*, 972-978. 10.1039/c3lc50959a
(30) Lagunas, A.; Comelles, J.; Martínez, E.; Samitier, J. Universal chemical gradient platforms using poly(methyl methacrylate) based on the biotin-streptavidin interaction for biological applications. *Langmuir* **2010**, *26*, 14154-14161. 10.1021/la102640w
(31) Weber, M.; Hauschild, R.; Schwarz, J.; Moussion, C.; Vries, I. d.; Legler, D. F.; Luther, S. A.; Bollenbach, T.; Sixt, M. Interstitial dendritic cell guidance by haptotactic chemokine gradients. *Science* **2013**, *339*, 328-332. 10.1126/science.1228456
(32) Cyster, J. G. Chemokines, sphingosine-1-phosphate, and cell migration in secondary lymphoid organs. *Annu. Rev. Immunol.* **2005**, *23*, 127-159. 10.1146/annurev.immunol.23.021704.115628
(33) Kawahara, M.; Hitomi, A.; Nagamune, T. Antigen-responsive regulation of cell motility and migration via the signalobodies based on c-Fms and c-Mpl. *Biotechnol. Prog.* **2014**, *30*, 411-417. 10.1002/btpr.1861
(34) Lagunas, A.; Comelles, J.; Martínez, E.; Prats-Alfonso, E.; Acosta, G. A.; Albericio, F.; Samitier, J. Cell adhesion and focal contact formation on linear RGD molecular gradients: Study of non-linear concentration dependence effects. *Nanomedicine* **2012**, *8*, 432-439. 10.1016/j.nano.2011.08.001

(35) Comelles, J.; Hortigüela, V. n.; Samitier, J.; Martínez, E. Versatile gradients of covalently bound proteins on microstructured substrates. *Langmuir* **2012**, *28*, 13688-13697. 10.1021/la3025638
(36) Wei, C.; Wang, X.; Zheng, M.; Cheng, H. Calcium gradients underlying cell migration. *Curr. Opin. Cell Biol.* **2012**, *24*, 254-261. 10.1016/j.ceb.2011.12.002
(37) Dickinson, R. B.; Tranquillo, R. T. Optimal estimation of cell movement indices from the statistical analysis of cell tracking data. *AIChE Journal* **1993**, *39*, 1995-2010. 10.1002/aic.690391210
(38) Caserta, S.; Campello, S.; Tomaiuolo, G.; Sabetta, L.; Guido, S. A methodology to study chemotaxis in 3-D collagen gels. *AIChE Journal* **2013**, *59*, 4025-4035. 10.1002/aic.14164
(39) Gorelashvili, M.; Emmert, M.; Hodeck, K. F.; Heinrich, D. Amoeboid migration mode adaption in quasi-3D spatial density gradients of varying lattice geometry. *New J. Phys.* **2014**, *16*, 075012. 10.1088/1367-2630/16/7/075012
(40) Ascione, F.; Caserta, S.; Perris, R.; Guido, S. Investigation of cell dynamics in vitro by time lapse microscopy and image analysis. *Chem. Eng. Trans.* **2014**, *38*, 517-522. 10.3303/CET1438087
(41) Griffith, L. G.; Naughton, G. Tissue engineering - current challenges and expanding opportunities. *Science* **2002**, *295*, 1009-1016. 10.1126/science.1069210
(42) Seras-Franzoso, J.; Peebo, K.; García-Fruitós, E.; Vázquez, E.; Rinas, U.; Villaverde, A. Improving protein delivery of fibroblast growth factor-2 from bacterial inclusion bodies used as cell culture substrates. *Acta Biomater.* **2014**, *10*, 1354-1359. 10.1016/j.actbio.2013.12.021
(43) Tatkiewicz, W. I.; Seras-Franzoso, J.; García-Fruitós, E.; Vazquez, E.; Ventosa, N.; Peebo, K.; Ratera, I.; Villaverde, A.; Veciana, J. Two-dimensional microscale engineering of protein-based nanoparticles for cell guidance. *ACS Nano* **2013**, *7*, 4774-4784. 10.1021/nn400907f
(44) Seras-Franzoso, J.; Peebo, K.; Corchero, J. L.; Tsimbouri, P. M.; Unzueta, U.; Rinas, U.; Dalby, M. J.; Vazquez, E.; Garcia-Fruitos, E.; Villaverde, A. A nanostructured bacterial bioscaffold for the sustained bottom-up delivery of protein drugs. *Nanomedicine* **2013**, *8*, 1587-1599. 10.2217/nnm.12.188
(45) Rinas, U.; Garcia-Fruitós, E.; Corchero, J. L.; Vázquez, E.; Seras-Franzoso, J.; Villaverde, A. Bacterial inclusion bodies: Discovering their better half. *Trends Biochem. Sci.* **2017**, *42*, 727-737. 10.1016/j.tibs.2017.01.005
(46) Unzueta, U.; Cespedes, M. V.; Sala, R.; Alamo, P.; Sánchez-Chardie, A.; Pesarrodona, M.; Sánchez-García, L.; Cano-Garrido, O.; Villaverde, A.; Vázquez, E.; Mangues, R.; Seras-

Franzoso, J. Release of targeted protein nanoparticles from functional bacterial amyloids: A death star-like approach. *J. Control. Release* **2018**, *279*, 29-39. 10.1016/j.jconrel.2018.04.004
(47) Céspedes, M. V.; Fernández, Y.; Unzueta, U.; Mendoza, R.; Seras-Franzoso, J.; Sánchez-Chardi, A.; Álamo, P.; Toledo-Rubio, V.; Ferrer-Miralles, N.; Vázquez, E.; Jr., S. S.; Abasolo, I.; Corchero, J. L.; Mangues, R.; Villaverde, A. Bacterial mimetics of endocrine secretory granules as immobilized in vivo depots for functional protein drugs. *Sci. Rep.* **2016**, *6*, 1-10. 10.1038/srep35765
(48) Loo, Y.; Goktas, M.; Tekinay, A. B.; Guler, M. O.; Hauser, C. A. E.; Mitraki, A. Self-assembled proteins and peptides as scaffolds for tissue regeneration. *Adv. Healthc. Mater.* **2015**, *4*, 2557-2586. 10.1002/adhm.201500402
(49) Stamm, A.; Strauß, S.; Vogt, P.; Scheper, T.; Pepelanova, I. Positive in vitro wound healing effects of functional inclusion bodies of a lipoxygenase from the mexican axolotl. *Microb. Cell Fact.* **2018**, *17*, 1-9. 10.1186/s12934-018-0904-0
(50) Tatkiewicz, W. I.; Seras-Franzoso, J.; Garcia-Fruitós, E.; Vazquez, E.; Kyvik, A. R.; Guasch, J.; Villaverde, A.; Veciana, J.; Ratera, I. Surface-bound gradient deposition of protein nanoparticles for cell motility studies. *ACS Appl. Mater. Interfaces* **2018**, *10*, 25779-25786. 10.1021/acsami.8b06821
(51) Macarron, R.; Banks, M. N.; Bojanic, D.; Burns, D. J.; Cirovic, D. A.; Garyantes, T.; Green, D. V. S.; Hertzberg, R. P.; Janzen, W. P.; Paslay, J. W.; Schopfer, U.; Sittampalam, G. S. Impact of high-throughput screening in biomedical research. *Nat. Rev. Drug Discov.* **2011**, *10*, 188-195. 10.1038/nrd3368
(52) He, Q.; Okajima, T.; Onoe, H.; Subagyo, A.; Sueoka, K.; Kuribayashi-Shigetomi, K. Origami-based self-folding of co-cultured NIH/3T3 and HEPG2 cells into 3D microstructures. *Sci. Rep.* **2018**, *8*, 4556. 10.1038/s41598-018-22598-x
(53) Bhardwaj, G.; Webster, T. J. Increased NIH 3T3 fibroblast functions on cell culture dishes which mimic the nanometer fibers of natural tissues. *Int. J. Nanomed.* **2015**, *10*, 5293-5299. 10.2147/IJN.S83007
(54) Rejmontová, P.; Capáková, Z.; Mikušová, N.; Maráková, N.; Kašpárková, V.; Lehocký, M.; Humpolíček, P. Adhesion, proliferation and migration of NIH/3T3 cells on modified polyaniline surfaces. *Int. J. Mol. Sci.* **2016**, *17*, 1439. 10.3390/ijms17091439